Artificial magnetic conductors realised by frequency-selective surfaces on a grounded dielectric slab for...

Article *in* IEE Proceedings - Microwaves Antennas and Propagation · November 2006

DOI: 10.1049/ip-map:20050156 · Source: IEEE Xplore

CITATIONS
44

READS
121

3 authors, including:

Alexander B. Yakovlev
University of Mississippi
214 PUBLICATIONS **2,090** CITATIONS
SEE PROFILE

Ahmed Kishk
Concordia University Montreal
676 PUBLICATIONS **9,323** CITATIONS
SEE PROFILE

Artificial magnetic conductors realised by frequency-selective surfaces on a grounded dielectric slab for antenna applications

M.A. Hiranandani, A.B. Yakovlev and A.A. Kishk

Abstract: New designs of artificial magnetic conductors (AMC), including hard and soft surfaces and dual-polarised high-impedance surfaces are realised by printed dipole/slot frequency-selective surfaces (FSS) implemented on a grounded dielectric slab. Multiband designs of hard and soft surfaces are proposed based on the use of FSS structures with different resonance lengths and orientation of dipoles/slots. In addition, dual-polarised high-impedance surfaces are realised by FSS structures with elements of different shapes (cross, loop), which create high impedance for both TE and TM polarisations. Commercial software EMPiCASSO is used for the fullwave analysis of presented FSS configurations. A printed slot FSS is proposed for design of a low-profile monopole antenna. The simulation and experimental results of return loss and radiation patterns are presented, demonstrating the effect of a high-impedance surface on scattering and radiation characteristics of a low-profile antenna.

1 Introduction

Artificial hard and soft surfaces, recently introduced in electromagnetics [1], are characterised by surface anisotropic impedance with respect to the propagation of surface waves [2]. Different approaches have been used for the realisation of hard and soft surfaces. Traditionally, they are realised by dielectric-filled corrugations initially proposed in the design of corrugated horn antennas [3, 4]. Another common method is to introduce perfect electric conductor (PEC) strips on a dielectric slab of certain thickness [5–9]. The main characteristics of such strip-loaded surfaces can be modelled by using an ideal model, which represents alternating PEC and PMC strips with vanishing widths [2], [10–12]. These anisotropic surfaces are polarisation-dependent, such that the hard surface behaves like a PMC for TE-polarised waves and as a PEC for TM-polarised waves propagating along the strips (corrugations). Alternatively, the soft surface behaves like a PEC for TE-polarised waves and as a PMC for TM-polarised waves propagating in the direction transverse to strips (corrugations) [2].

New designs of artificial hard and soft surfaces composed of printed dipole/slot FSS structures on a grounded dielectric slab have been recently presented in [13, 14] (Fig. 1). These FSS structures represent AMC surfaces with anisotropic impedance characteristics controlled by the resonance properties of periodic dipole/slot cells in the presence of a grounded dielectric slab. Multiband designs of such AMC surfaces have also been presented in [15, 16] where multiple dipoles of different lengths are used to obtain multiple resonances. They are implemented on electrically-thin substrates (compared to the electrically-thick substrates used in the strip-loaded hard and soft surfaces discussed above), which make them attractive for low-profile antenna applications.

These printed dipole/slot FSS structures act as hard and soft surfaces in a certain frequency band. For a plane wave incident in the direction perpendicular to dipoles, this structure performs as a hard surface exhibiting PMC behaviour for TE polarisation, while for TM-polarised plane waves there is no interaction with the dipoles exhibiting nearly PEC behaviour (very low surface impedance). When the plane wave is incident in the direction of dipoles, the structure exhibits high impedance for TM polarisation and low impedance for TE polarisation, thus acting as a soft surface. On the other hand, slot FSS produces the opposite behaviour with respect to TE and TM polarisations. However, it should be noted that the length of slots in the proposed FSS is greater with respect to the length of dipoles in order to resonate at the same frequency. Here we are dealing with two different periodic structures, one with electric current on a dielectric interface backed by a PEC ground plane, and the other with slots backed by a PEC ground plane, and these two structures

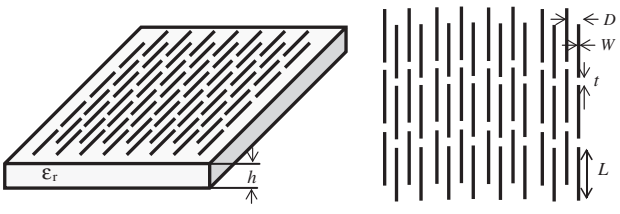

Fig. 1 *Hardlsoft Gangbuster surface realised by printed dipoles (slots) on a grounded dielectric slab*

IEE Proceedings online no. 20050156

doi:10.1049/ip-map:20050156

Paper first received 2nd July 2005 and in revised form 14th February 2006

M.A. Hiranandani is with the Mobile Wireless Group, Intel Corporation, 5200 Elam Young Parkway, Hillsboro, OR 97124, USA

A.B. Yakovlev and A.A. Kishk are with the Department of Electrical Engineering, Center for Applied Electromagnetic Systems Research (CAESR), University of Mississippi, University, MS 38677-1848, USA

E-mail: manish.a.hiranandani@intel.com

are not dual to each other since dual to a slot on a PEC would be an electric current (dipole) on a perfect magnetic conductor (PMC). A FSS with a given length of dipole or slot will have different resonant frequencies because the effective dielectric constant for both the structures is different. For the slot case, the effective dielectric constant is equal to the relative dielectric constant, but in the dipole case the effective dielectric constant is less than the relative dielectric constant.

The results reported in [13] for printed dipole/slot FSS (Figs. 3 and 5 in [13]) have been verified using commercial software EMPiCASSO [17], showing an excellent agreement for the case of hard and soft slots (Fig. 5 in [13]). In the case of hard and soft dipoles (Fig. 3 in [13]), a shift in the resonance frequency is observed (EMPiCASSO results are in the range of frequencies 8.12–8.16 GHz against 7.78–7.82 GHz presented in [13]). The plotted results for these cases are omitted here for brevity.

Based on the idea presented in [13] and discussed above, here we propose new designs of multiband hard and soft surfaces and dual-polarised FSS in order to create a high impedance surface. Multiband hard and soft surfaces are realised by FSS structures with different resonance lengths and orientation of dipoles/slots. FSS structures with elements of various shapes (cross, loop) are used to create dual-polarised high-impedance surfaces for both TE and TM polarisations. Commercial software EMPiCASSO [17] is used for the fullwave analysis of the proposed FSS configurations. A printed slot FSS is proposed for the design of a low-profile monopole antenna, which is simulated by using the Ansoft high-frequency structure simulator (HFSS) commercial program [18]. The simulation and experimental results of return loss and radiation pattern are presented, demonstrating the effect of a high impedance surface on scattering and radiation characteristics of a low-profile antenna.

2 Multiband printed dipole FSS structures

2.1 Dual-band design

The importance of dual-band FSS designs was established during NASA's Cassini project, where dual subreflectors were used as feeds for the main reflector operating at two desired bands [19]. Also, in [15] and [16] it was proposed to use more than one element in a single unit cell of FSS in order to create multiband AMC surfaces. This idea is applied here in the design of dual-band hard and soft surfaces using printed dipole FSS implemented on a grounded dielectric slab (Fig. 2*a*), wherein two dipoles of different resonance lengths are considered in a unit cell (Fig. 2*b*), instead of a single dipole unit cell used in the initial design (Fig. 1). The dispersion behaviour of the phase of the reflection coefficient is shown in Fig. 3 for a TM-polarised plane wave with normal incidence. Two resonances around 8 GHz and 14 GHz corresponding to different lengths of two dipoles are associated with the high-impedance surface boundary condition (PMC surface with no phase reversal). With the plane of incidence in the direction of dipoles (as shown in Fig. 2*a*), the TE polarisation does not interact with the structure, thus showing the behaviour of the phase of the reflection coefficient for the grounded dielectric slab; the TE polarisation in this case does not 'see' the dipoles and the phase behaviour is close to that for the PEC (ground plane with a thin dielectric slab). The TM polarisation, however, strongly interacts with the structure and exhibits the high-impedance surface behaviour. It should be noted that the resonance frequencies of the dual-band FSS are mainly

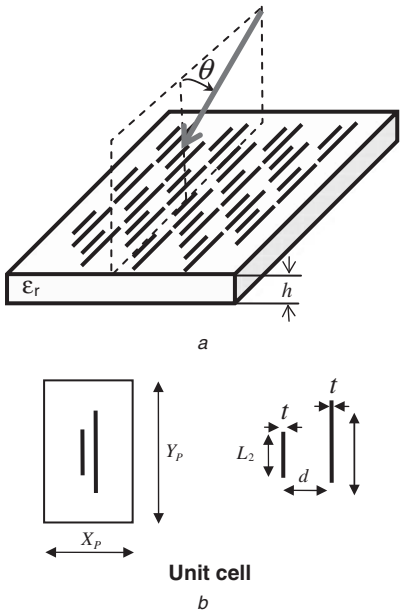

Fig. 2 *Printed dipole FSS for dual-band operation*
a General view of the structure showing the direction of wave propagation
b Unit cell
All dimensions are in mm, $t = 0.25$, $d = 2.514$, $h = 1$, $\varepsilon_r = 4$, $L_1 = 10$, $L_2 = 6$, $X_p = 5.127$, $Y_p = 10.25$, and $Y_{offset} = 3.95$

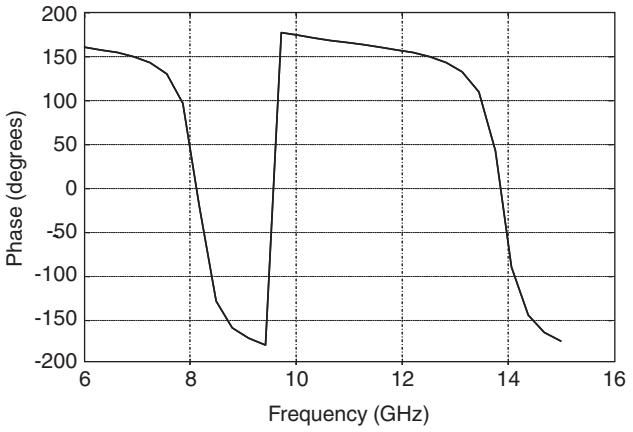

Fig. 3 *Dispersion behaviour of the phase of the reflection coefficient for TM-polarised plane wave with normal incidence on the dual-band printed dipole FSS (Fig. 2)*
Two resonances associated with the high-impedance surface appear around 8 GHz and 14 GHz

determined by the length of dipoles, which indicates that the coupling among the dipoles, which is included in the fullwave simulation, does not have a significant effect on the resonance frequencies, contrary to the slot case.

The results for the phase of the reflection coefficient against the angle of incidence θ (defined in Fig. 2*a*) are demonstrated in Figs. 4*a* and 4*b*. As is seen in Fig. 4*a*, the phase of the reflection coefficient of the longer dipole behaves similarly to that of the initial design [13], while the phase of the shorter dipole varies insignificantly producing high impedance for a wide range of the incident angle (Fig. 4*b*). The resonance properties of the proposed dual-band FSS structure are primarily due to resonance properties of two dipoles, exhibiting two distinct resonances corresponding to resonance lengths of the dipoles. In this

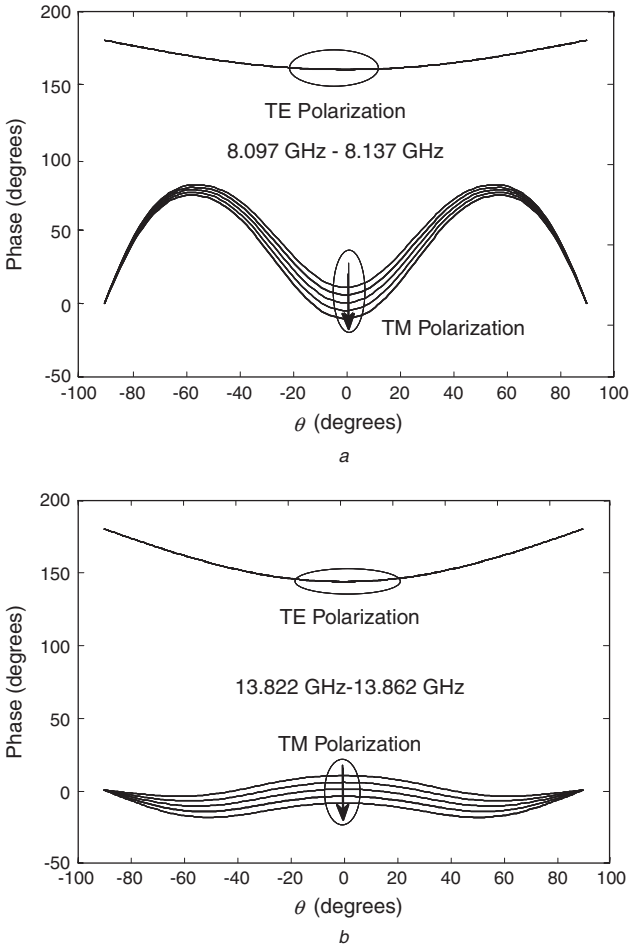

Fig. 4 *Resonance of two dipoles in the dual-band design*
a The longer dipole
b The shorter dipole
The arrow indicates the increase of frequency with the increment of 8 MHz

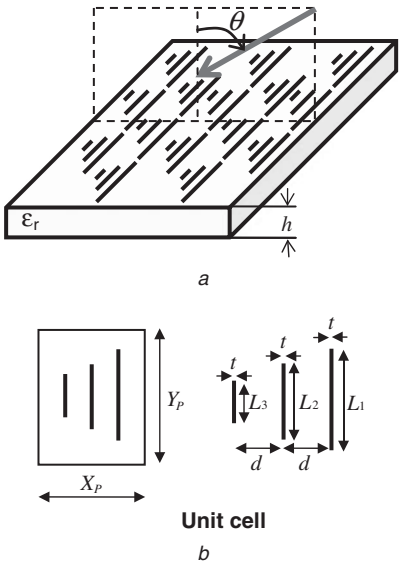

Fig. 5 *Printed dipole FSS for triple-band operation*
a General view of the structure showing the direction of wave propagation
b Unit cell
All dimensions are in mm, $t = 0.25$, $d = 1.282$, $h = 1$, $\varepsilon_r = 4$, $L_1 = 10$, $L_2 = 8$, $L_3 = 6$, $X_p = 5.127$, $Y_p = 10.25$, and $Y_{offset} = 3.95$

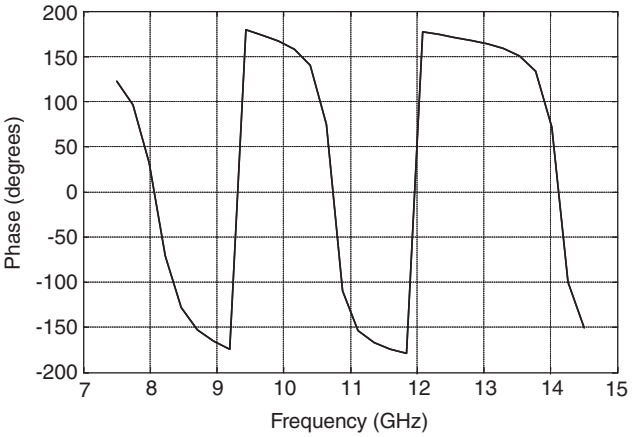

Fig. 6 *Dispersion behaviour of the phase of the reflection coefficient for TE-polarised plane wave with normal incidence on the triple-band printed dipole FSS (Fig. 5)*
Three resonances associated with the high-impedance surface appear around 8, 10.7 and 14 GHz

case when the plane of incidence is along the dipoles (as shown in Fig. 3) the structure acts as a high impedance surface for TM polarisation and as a low impedance surface for TE polarisation. It should be noted that there is no 'perfect' soft (hard) surface realised by printed dipole FSS on a grounded dielectric slab according to the traditional definition of soft (hard) surfaces in terms of PEC and PMC boundary conditions.

2.2 Triple-band design

The triple-band FSS structure is composed of periodic cells of three dipoles with different lengths corresponding to three resonance frequencies (Fig. 5). In the case when the plane of incidence is perpendicular to dipoles (as shown in Fig. 5*a*), the role of TE and TM polarisations is interchanged in comparison with the previous case of dual-band design. In this case, the TE polarisation exhibits a high-impedance behaviour and the TM polarisation exhibits a low-impedance behaviour. The dispersion behaviour of the phase of the reflection coefficient for a TE-polarised plane wave with normal incidence is shown in Fig. 6, where three distinct resonances appear around 8 GHz, 10.7 GHz and 14 GHz corresponding to the high-impedance boundary condition with no phase reversal (zero degrees in the phase of the reflection coefficient). It was expected that the resonances of all these dipoles could be brought closer to each other by having dipoles of corresponding resonant lengths to exhibit a broad-band design, similar to the technique used in the design of Yagi Uda antennas. However, it was noticed that the triple-band structure behaved as three independent frequency-selective surfaces, maintaining three distinct resonances.

The results for the phase of the reflection coefficient against the angle of incidence θ are demonstrated in Figs. 7*a* and 7*b*. In this case, the TM polarisation does not interact with the structure, thus showing the behaviour of the phase of the reflection coefficient for the grounded dielectric slab. The TE polarisation, however, strongly interacts with the structure and exhibits the high-impedance surface behaviour. It should be noted that the proposed multiband designs of printed dipole FSS structures can be realised by printed slot FSS on a grounded dielectric slab, with opposite behaviour with respect to TE and TM polarisations (the results are omitted) here due to space limitations).

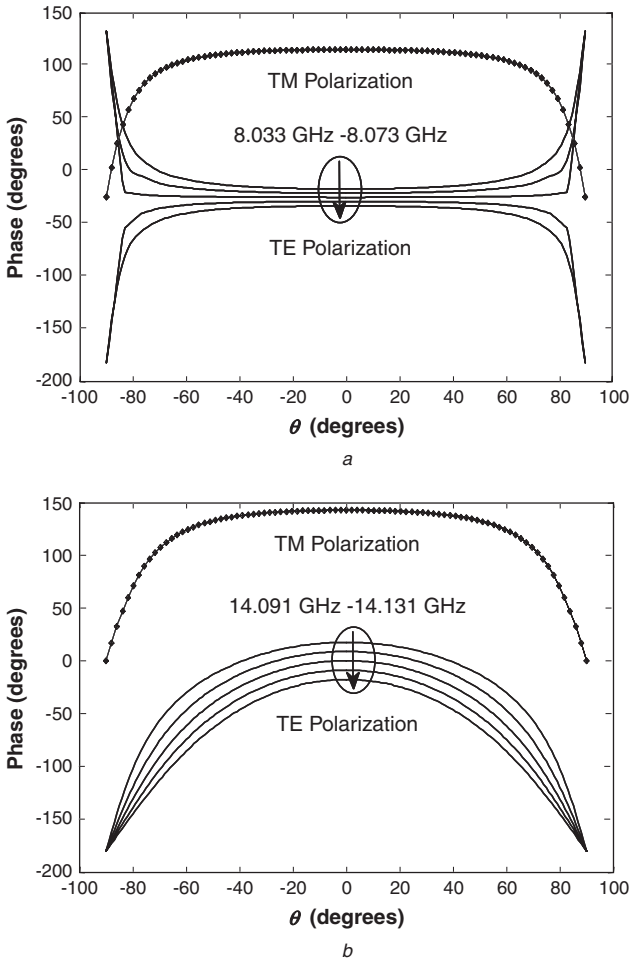

Fig. 7 *Resonance of two dipoles in the triple-band design*
a The longest dipole in the triple-band design
b The shortest dipole
The arrow indicates the increase of frequency with the increment of 8 MHz

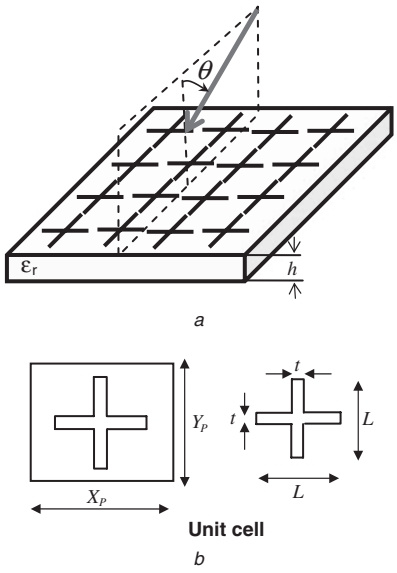

Fig. 8 *Dual-polarised cross-shaped slot FSS on a grounded dielectric slab*
a General view of the structure showing the direction of wave propagation
b Unit cell
All dimensions are in mm, $L = 10$, $t = 0.25$, $h = 1$, $\varepsilon_r = 4$ and $X_p = Y_p = 10.5$

3 Dual-polarised high-impedance surfaces

3.1 Cross-shaped slot FSS

In the method discussed above, replacing the narrow dipole/slot by a cross-shaped dipole/slot provides polarisation independence with respect to the TE and TM incidence. The design presented in Fig. 8 is that of a cross-shaped slot. The dispersion behaviour of the phase of the reflection coefficient for a TE-polarised plane wave with the normal incidence is shown in Fig. 9. It can be seen that the structure experiences a PMC behaviour at 9.29 GHz with a high-impedance boundary condition with 3.7% bandwidth when the phase of the reflection coefficient varies between -90° and $+90^\circ$. With the direction of propagation as shown in Fig. 8, the TE polarisation excites the vertical slot and the TM polarisation excites the horizontal slot. Hence, this structure exhibits high-impedance irrespective of TE or TM polarisation as shown in Fig. 10. The proposed cross-shaped FSS behaves as a dual-polarised PMC surface for normal incidence and as a dual-polarised high-impedance-surface for oblique incidence.

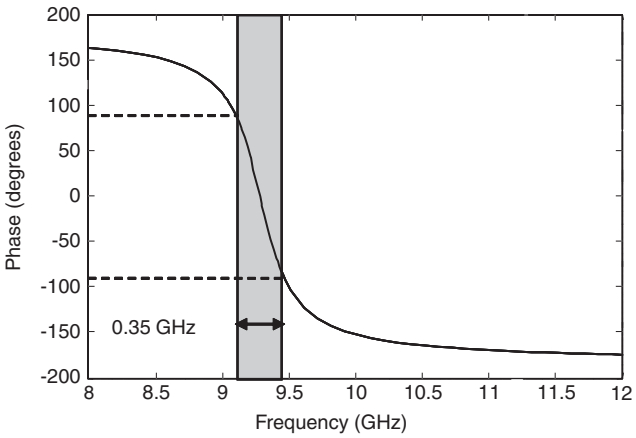

Fig. 9 *Dispersion behaviour of the phase of the reflection coefficient for a TE-polarised plane wave with normal incidence on the cross-shaped slot FSS*

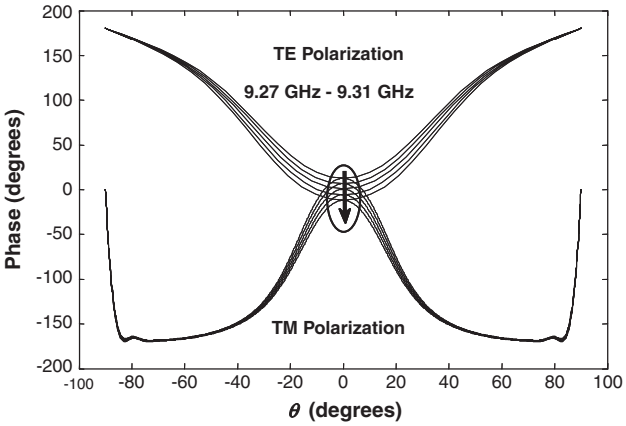

Fig. 10 *Resonance behaviour of vertical and horizontal slots in the cross-shaped FSS against the angle of incidence*
The arrow indicates the increase of frequency with the increment of 8 MHz

3.2 Rectangular-loop slot FSS

The above discussed configurations of multiband printed dipole FSS and dual-polarised cross-shaped slot FSS act as high-impedance surfaces in a narrow frequency band (see Figs. 3, 6 and 9 for rapid variation of the phase of reflection

coefficient around the resonance frequencies). Here, we propose to use rectangular loops in order to create a wideband high-impedance slot FSS structure with dual polarisation. The geometry of the structure with its unit cell is shown in Fig. 11. The dispersion behaviour of the phase of the reflection coefficient for a TE-polarised plane wave with the normal incidence is shown in Fig. 12. It can be seen that the structure experiences a PMC behaviour at 10 GHz with a high-impedance boundary condition of 12.5% bandwidth when the phase of the reflection coefficient varies between -90° and $+90^\circ$ (compare with 3.7% bandwidth of cross-shaped slot FSS considered in the previous section). The results for TE and TM polarisations against the angle of incidence are shown in Fig. 13, where both polarisations result in a PMC boundary condition for a wide range of the incident angle.

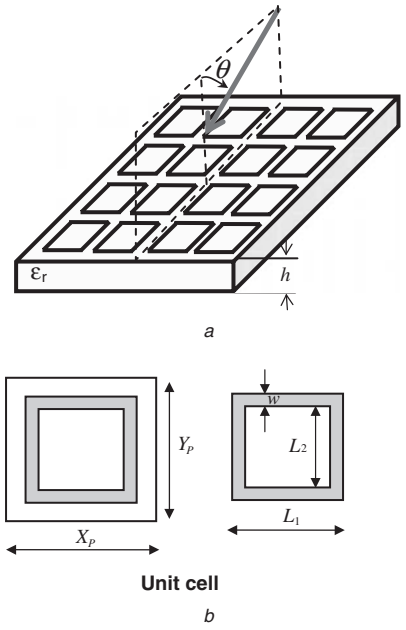

Fig. 11 *Dual-polarised rectangular-loop slot FSS on a grounded dielectric slab*
a General view of the structure showing the direction of wave propagation
b Unit cell
All dimensions are in mm, $w = 0.45$, $L_1 = 4.672$, $L_2 = 3.772$, $h = 1.28$, $\varepsilon_r = 10.2$ and $X_p = Y_p = 5$

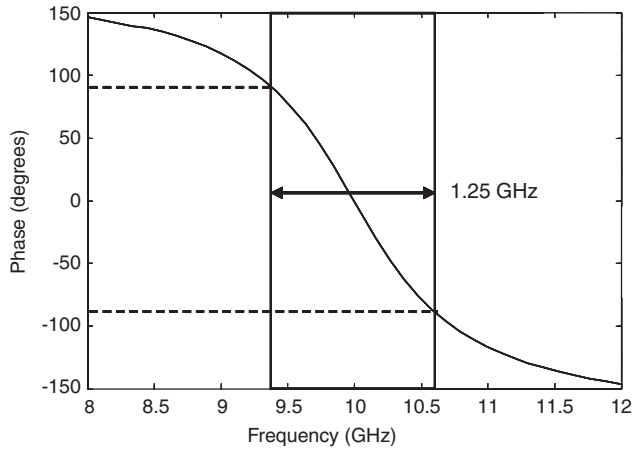

Fig. 12 *Dispersion behaviour of the phase of the reflection coefficient for a TE-polarised plane wave with normal incidence on the rectangular loop slot FSS*

3.3 Circular-loop slot FSS

In addition to the rectangular-loop configuration presented in the previous section, a circular-loop wideband design is proposed for a dual-polarised slot FSS structure (with geometry shown in Fig. 14). The dispersion behaviour of the phase of the reflection coefficient for a TE-polarised plane wave with normal incidence is shown in Fig. 15. It can be seen that the structure experiences a PMC behaviour at 10 GHz with a high-impedance boundary condition of 7.8% bandwidth when the phase of the reflection coefficient varies between -90° and $+90^\circ$. It behaves similar to the rectangular-loop FSS with a slightly narrower bandwidth. The results for TE and TM polarisations against the angle of incidence are shown in Fig. 16, where both polarisations result in a PMC boundary condition for a wide range of the incident angle.

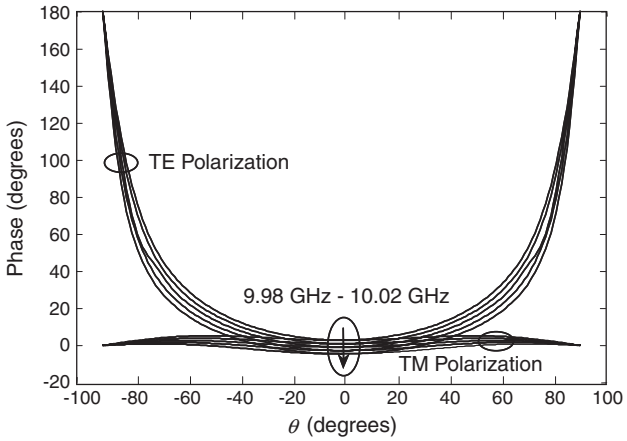

Fig. 13 *Resonance behaviour of rectangular loops in dual-polarised slot FSS against the angle of incidence*
The arrow indicates the increase of frequency with the increment of 8 MHz

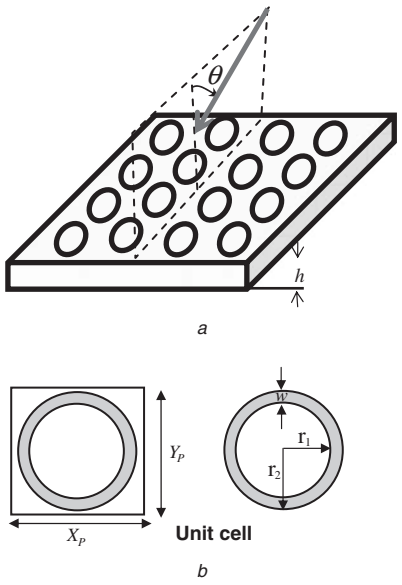

Fig. 14 *Dual-polarised circular-loop slot FSS on a grounded dielectric slab*
a General view of the structure showing the direction of wave propagation
b Unit cell
All dimensions are in mm, $w = 0.1225$, $r_1 = 2.3275$, $r_2 = 2.45$, $h = 1.28$, $\varepsilon_r = 10.2$ and $X_p = Y_p = 5.5$

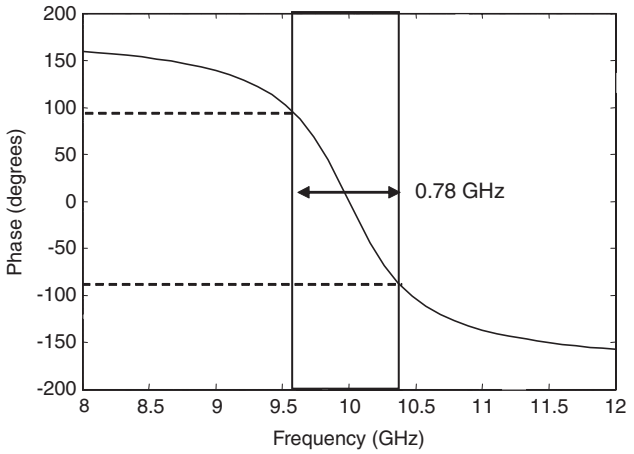

Fig. 15 *Dispersion behaviour of the phase of reflection coefficient for a TE-polarised plane wave with normal incidence on the circular-loop slot FSS*

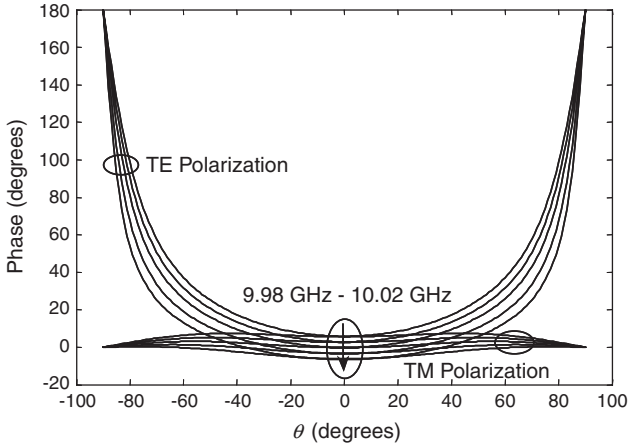

Fig. 16 *Resonance behaviour of circular-loops in dual-polarised slot FSS against the angle of incidence*
The arrow indicates the increase of frequency with the increment of 8 MHz

4 Low-profile monopole antenna: design and experiment

Recently, high-impedance surfaces (in particular, electromagnetic band-gap (EBG) mushroom-like structures) have been used in low-profile antenna designs in order to suppress surface waves and enhance the antenna radiation [20–22]. Here, we propose to use the above discussed printed FSS as a high-impedance surface to improve the performance of low-profile antennas. A slot FSS, printed on a grounded dielectric slab (RO4003C, Roger's Corporation) of thickness 0.813 mm with permittivity 3.38, was designed at the frequency of 10 GHz. A quarter-wavelength horizontal monopole was used as a radiator placed in close proximity (1.2 mm) to the slot FSS acting as an artificial magnetic conductor (AMC) at the resonance frequency. The slot FSS consists of an array of 5×10 cells of printed slots of dimensions 16×0.5 mm with the cell size 16.4×8.19 mm. This structure (horizontally-bended monopole above the slot FSS) was simulated using Ansoft HFSS [18] and a prototype was fabricated. A photograph of the fabricated FSS with the mounted monopole is shown in Fig. 17. The simulation and experimental results of return loss of the monopole in the presence of AMC compared to those over PEC are shown in Fig. 18. It is clear that the monopole (of length 9 mm) is matched in the case of AMC at approximately 10.0 GHz (around the resonance frequency of the slot FSS) and is mismatched in the case of PEC resulting in poor radiation characteristics of the monopole antenna.

The simulated and measured radiation patterns of the monopole mounted on the above designed structure were compared with the radiation patterns of the same antenna over PEC. The idea was to compare the results to see the effect of the presence of AMC on the performance of such a low-profile antenna. The simulated and measured E-plane radiation patterns are plotted in Figs. 19 and 20, respectively. When the antenna is mounted on a PEC, its front-side radiation pattern is almost uniform as it radiates the power equally in all directions. Comparing this pattern with the pattern of the same antenna over the AMC shows that the AMC pattern has a power level of 6–10 dB higher than the PEC pattern. This shows that the AMC surface enhances the gain of the horizontal monopole as compared

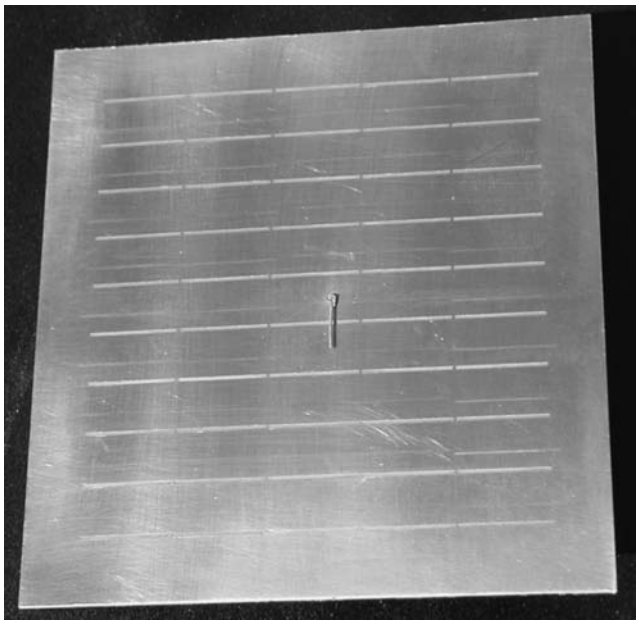

Fig. 17 *Photograph of the printed slot FSS for design of a low-profile monopole antenna*

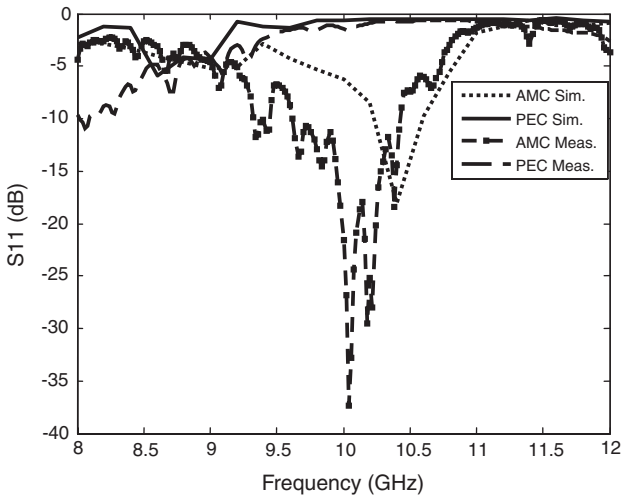

Fig. 18 *Simulated and measured results of return loss of the horizontal monopole mounted in close proximity to the AMC and PEC*

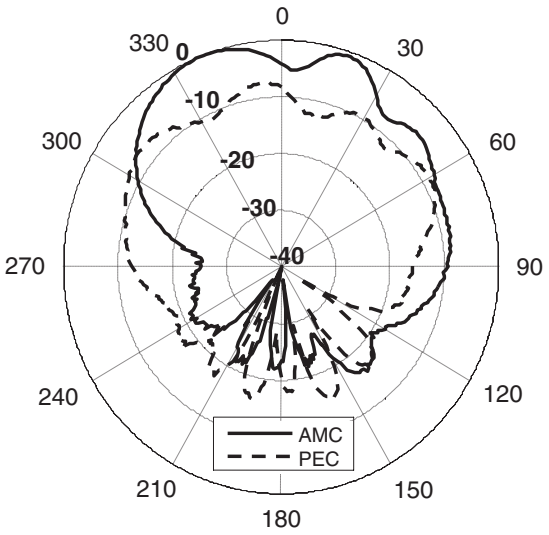

Fig. 19 *Simulated radiation patterns of the horizontal monopole mounted on AMC and PEC surfaces*

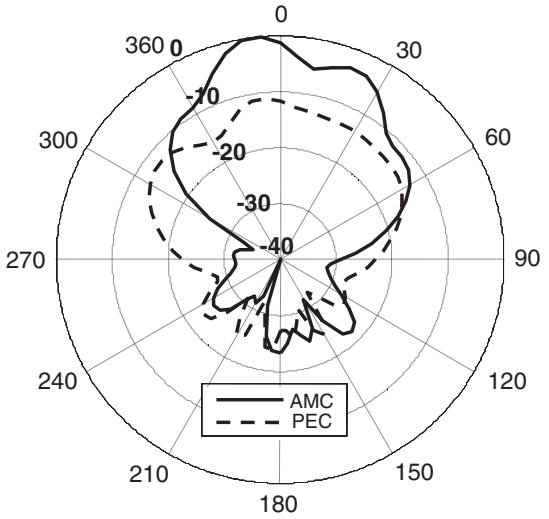

Fig. 20 *Measured radiation patterns of the horizontal monopole mounted on AMC and PEC surfaces*

to its inefficient radiation in the presence of the PEC (due to reversed image currents).

5 Conclusions

In this paper, different designs of AMC structures, including hard and soft surfaces and dual-polarised high-impedance surfaces are realised by printed dipole/slot FSS on a grounded dielectric slab. Dual-band and triple-band printed dipole FSS structures are studied, and cross-shaped, rectangular-and circular-loop printed slot FSS are analysed to create a dual-polarised high-impedance surface for both TE and TM polarisations. It is shown that rectangular (circular) loops used in printed slot FSS result in dual-polarised wideband high-impedance surfaces. The printed slot FSS as a high-impedance ground plane is proposed in the design of a low-profile monopole antenna. The FSS structure with the monopole (mounted in a close proximity) was designed, fabricated and measured, showing the enhancement of radiation for the low-profile antenna.

6 Acknowledgments

This work was partially supported by the National Science Foundation under Grant ECS-0220218 and NASA EPS-CoR Cooperative Agreement NCC5-574. The authors are greatful to Dr. R. Chair from the University of Mississippi for helping with measurements.

7 References

1 Kildal, P.-S.: 'Artificially soft and hard surfaces in electromagnetics', *IEEE Trans. Antennas Propag.*, 1990, **38**, (10), pp. 1537–1544
2 Kildal, P.-S., and Kishk, A.A.: 'EM modeling of surfaces with STOP or GO characteristics – artificial magnetic conductors and soft and hard surfaces'. Proc. 19th Annual Review of Progress in Applied Computational Electromagnetics, Monterey, CA, USA, March 2003, pp. 445–455
3 Kildal, P.-S.: 'Definition of artificially soft and hard surfaces for electromagnetic waves', *Electron. Lett.*, 1988, **24**, (3), pp. 168–170
4 Kildal, P.-S.: 'Technical memorandum: bandwidth of a square hard horn', *IEE Proc. H, Microw. Antennas Propag.*, 1988, **135**, (4), pp. 275–278
5 Lier, E.: 'Analysis of soft and hard strip-loaded horns using a circular cylindrical model', *IEEE Trans. Antennas Propag.*, 1990, **38**, (6), pp. 783–793
6 Kishk, A.A., and Morgan, M.: 'Analysis of circular waveguides with soft and hard surfaces realized by strip-loaded walls using asymptotic boundary conditions', *Microw. Opt. Technol. Lett.*, 2001, **29**, (6), pp. 433–436
7 Kishk, A.A., and Kildal, P.-S.: 'Asymptotic boundary conditions for strip-loaded scatterers applied to circular dielectric cylinders under oblique incidence', *IEEE Trans. Antennas Propag.*, 1997, **45**, (1), pp. 51–56
8 Kishk, A.A.: 'Analysis of hard surfaces of cylindrical structures of arbitrarily shaped cross section using asymptotic boundary conditions', *IEEE Trans. Antennas Propag.*, 2003, **51**, (6), pp. 1150–1156
9 Simon, A.E., and Kishk, A.A.: 'Asymptotic strip boundary condition in the finite difference time domain method', *IEEE Trans. Antennas Propag.*, 2005, **53**, (3), pp. 1187–1193
10 Ruvio, G., Kildal, P.-S., and Maci, S.: 'Modal propagation in ideal soft and hard surface'. IEEE AP-S Int. Symp., Columbus, OH, USA, June 2003, pp. 438–441
11 Klymko, V.A., Yakovlev, A.B., Eshrah, I.A., Kishk, A.A., and Glisson, A.W.: 'Dyadic Green's function of an ideal hard surface circular waveguide with application to excitation and scattering problems', *Radio Sci.*, 2005, **40**, RS3014, doi:10.1029/2004RS003167
12 Huang, W., Yakovlev, A.B., Kishk, A.A., Glisson, A.W., and Eshrah, I.A.: 'Green's function analysis of an ideal hard surface rectangular waveguide', *Radio Sci.*, 2005, **40**, RS5006, doi:10.1029/2004RS003161
13 Maci, S., and Kildal, P.-S.: 'Hard and soft Gangbuster surfaces'. Proc. URSI Int. Symp. Electromagnetic Theory, Pisa, Italy, May 2004, pp. 290–292
14 Maci, S., Caiazzo, M., Cucini, A., and Casaletti, M.: 'A pole-zero matching method for EBG surfaces composed of a dipole FSS printed on a grounded dielectric slab', *IEEE Trans. Antennas Propag.*, 2005, **53**, (1), pp. 70–81
15 Feresidis, A.P., Chauraya, A., Goussetis, G., Vardaxoglou, J.C., and deMaagt, P.: 'Multi-band artificial magnetic conductor surfaces'. IEE Seminar on Metamaterials for Microwave and (Sub) Millimeter Wave Applications: Photonic Band gap and Double Negative Designs, Components and Experiments, 23 Nov. 2003, pp. 2/1–2/6
16 Goussetis, G., Guo, Y., Feresidis, A.P., and Vardaxoglou, J.C.: 'Miniaturized and multi-band artificial magnetic conductors and electromagnetic band gap surfaces'. IEEE Antennas Propagation Society Int. Symp., 20-25 June 2004, Vol. 1, pp. 293–296
17 EMPiCASSO: User's Manual, EMAG Technologies, Inc, 2002
18 HFSS: High frequency structure simulator based on the finite element method, v. 9.2.1, Ansoft Corporation, 2004
19 Wu, T.K.: 'Four-band frequency selective surface with double-square-loop patch elements', *IEEE Trans. Antennas Propag.*, 1994, **42**, (12), pp. 1659–1663
20 Liu, T.H., Zhang, W.X., Zhang, M., and Tsang, K.F.: 'Low profile spiral antenna with PBG substrate', *Electron. Lett.*, 2000, **36**, (9), pp. 779–780
21 Yang, F., and Rahmat-Samii, Y.: 'A low profile circularly polarized curl antenna over electromagnetic band-gap (EBG) surface', *Microw. Opt. Technol. Lett.*, 2001, **31**, (3), pp. 165–168
22 Yang, F., and Rahmat-Samii, Y.: 'Reflection phase characterizations of the EBG ground plane for low profile wire antenna applications', *IEEE Trans. Antennas Propag.*, 2003, **51**, (10), pp. 2691–2703